

d-Wave Magnetism in Cuprates from Oxygen Moments

Ying Li,^{1,2,*} Valentin Leeb,^{1,3,*} Krzysztof Wohlfeld,⁴ Roser Valentí,⁵ and Johannes Knolle^{1,3,6}

¹*Physics Department, Technical University of Munich,
TUM School of Natural Sciences, 85748 Garching, Germany*

²*MOE Key Laboratory for Nonequilibrium Synthesis and Modulation of Condensed Matter,
School of Physics, Xi'an Jiaotong University, Xi'an 710049, China*

³*Munich Center for Quantum Science and Technology (MCQST), Schellingstr. 4, 80799 München, Germany*

⁴*Institute of Theoretical Physics, Faculty of Physics,
University of Warsaw, Pasteura 5, PL-02093 Warsaw, Poland*

⁵*Institut für Theoretische Physik, Goethe-Universität Frankfurt,
Max-von-Laue-Strasse 1, 60438 Frankfurt am Main, Germany*

⁶*Blackett Laboratory, Imperial College London, London SW7 2AZ, United Kingdom*
(Dated: December 17, 2024)

The antiferromagnetic parent phase of high- T_c cuprates has been established as a Néel state of copper moments, but early work pointed out the important role of ligand oxygen orbitals. Using the three-orbital Emery model we show how doping-induced antiferromagnetic ordering of weak magnetic moments on the oxygen sites can lead to unconventional d-wave magnetism with spin-split electronic bands. Our mechanism for forming such altermagnetic (AM) states in cuprates does not rely on a lowering of the crystal symmetry but rather on interaction-induced formation of magnetic moments on directional oxygen orbitals within the crystallographic unit cell. Therefore, we obtain two different types of AM, namely a (0,0)-AM and a (π,π) -AM, and identify different mechanisms for appearance supported by Hartree-Fock and exact diagonalization calculations. We finally suggest a scenario to realize the unconventional spin-split bands in a candidate compound by density functional theory and discuss experimental implications.

I. INTRODUCTION

Understanding the parent phase of cuprates has been key for elucidating the emergence of high- T_c superconductivity [1, 2]. The insulating parent Néel state is typically described as a commensurate antiferromagnet (AFM) of a single orbital model of magnetic moments on the copper sites [3–5]. However, early on Emery discussed the relevance of oxygen orbitals for understanding the magnetic fluctuations upon doping which are responsible for pairing [6]. Not only is the exchange between copper moments mediated via the directional p_x, p_y orbitals [6–10] but the position of oxygen on the bond centers leads to a unit cell with an internal structure which allowed for the prediction of intra-unit cell order, for example of spin nematic [11, 12] or loop current type [13, 14]. Neutron scattering experiments established the importance of the hybridization between oxygen and copper orbitals for understanding the magnetic form factors [15]. Famously, in the pseudo-gap phase neutron scattering measurements also observed magnetism without additional lattice symmetry breaking pointing to intra-unit cell order [16, 17], which was argued to be consistent with staggered magnetic moments of the oxygen sites.

Recently, a new type of collinear antiferromagnetism, so called altermagnetism (AM), has been proposed which combines spin-split electronic bands expected for ferromagnets (FM) with a vanishing net moment of AFMs [18–26]. The reason is the absence of translational

(or inversion) symmetry between the AFM sublattices, which can either originate from a low crystal symmetry or appear spontaneously from directional orbital ordering [27]. In the context of AMs, the cuprate La_2CuO_4 has been proposed as a candidate material [24, 28] arising from a reduced crystal symmetry due to the canting of CuO_6 octahedra. However, the resulting spin splittings are small and disappear when the structure becomes tetragonal under doping. In three-dimensional analogues of the parent compound $\text{CuAg}(\text{SO}_4)_2$, AM appears, again, because of crystallographically different Cu-Ag sublattices [29].

Here, we show that AM of the d -wave type can already appear in highly symmetric tetragonal CuO_2 planes from magnetic moments on directional oxygen orbitals. Typically, cuprates are modeled to have AFM moments on the Cu atoms, see upper right panel of Fig. 1. We investigate the possibility of additional AFM moments on the oxygen orbitals (lower panels), which can result in two distinct types of AM states: First, a (0,0)-AM which does not break any translational symmetry but leads to a spin splitting because of the intra-unit cell AFM arrangement. Second, a (π, π) -AM can appear where both Cu and O have AFM moments and the unit cell is spontaneously enlarged leading to a backfolding of the electronic bands (see right panels). The interesting point is that for both scenarios intra-unit cell oxygen AFMs is responsible for distinct spin-split electronic bands with a d -wave form factor as shown in the lower panels of Fig. 1.

We note that AM without translational symmetry breaking has been discussed previously [11, 30, 31] but here we concentrate on its microscopic origin in cuprates

* These two authors contributed equally

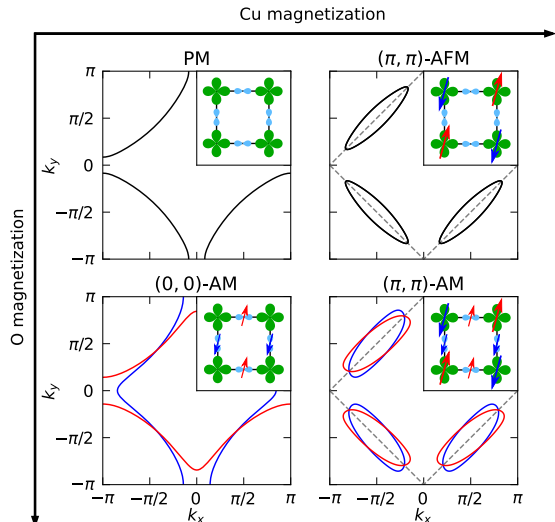


FIG. 1. Typically the AFM phase of cuprates feature AFM moments on the Cu atoms (x-axis). Here, we additionally explore the formation of AFM moments on the oxygen orbitals (y-axis), which leads to two different types of AM states. The insets of the subpanels show the possible magnetic phases we obtain (Cu green, O light blue). The subpanels show the spin resolved Fermi surface (FS) for the corresponding phase (black degenerate, red spin-up, blue spin-down). The magnetic Brillouin zone is shown as gray dashed square. Note that the lower left intra-unit cell ordering does not break translational symmetry as suggested in previous neutron scattering experiments [16, 17].

and its unique electronic properties. We identify three distinct microscopic mechanisms that could lead to the formation of magnetic moments on the oxygens: (i) A direct exchange between oxygen due to a large repulsive interaction U_p on oxygen sites; (ii) A strong charge transfer bringing the p -oxygen orbitals closer to the Fermi energy; and (iii) A large oxygen-oxygen hopping t_{pp} effectively shifting magnetic moments of copper to oxygens.

Our work is organized as follows. We explore the emergence and stability of distinct AM phases summarized in Fig.1 within the three-band Emery model, which we introduce in detail. We identify distinct mechanisms on how AFM correlations between oxygen moments can be stabilized, which we support by Hartree-Fock calculations and exact diagonalization of finite clusters. We then propose a potential cuprate material realizing AM using density functional theory. Finally, we discuss the unique experimental properties of the putative d -wave magnetism like anisotropic spin transport and splitting of spin wave branches observable via inelastic neutron scattering experiments.

II. ELECTRONIC STRUCTURE AND MODEL HAMILTONIAN.

All cuprates feature CuO_2 planes with Cu^{2+} ions in a $3d^9$ configuration with a localized hole in the Cu $3d_{x^2-y^2}$ orbital. The parent compounds are charge-transfer insulators [32], where the top of the band formed by the oxygen p_x, p_y orbitals is located above the lower Hubbard band. This is well captured within the three-band Emery model [6, 9, 10]. Under doping, holes transfer to the oxygen ligands and at large doping a metallic state emerges [33] which is also consistent with density functional theory (DFT) calculations [34–38].

In this work we concentrate on the three-band Emery model

$$\mathcal{H} = \sum_{i\mu\sigma} \epsilon_\mu n_{i\mu\sigma} + \sum_{i\mu j\nu\sigma} t_{i\mu j\nu} \mathbf{c}_{i\mu\sigma}^\dagger \mathbf{c}_{j\nu\sigma} + \sum_{i\mu} U_\mu n_{i\mu\uparrow} n_{i\mu\downarrow}, \quad (1)$$

where i, j label the square lattice unit cell, consisting of the $d_{x^2-y^2}$ Cu orbital ($\mu, \nu = d$) which is surrounded by O p_x and p_y orbitals ($\mu, \nu = p_x, p_y$). $\mathbf{c}_{i\mu\sigma}^\dagger$ ($\mathbf{c}_{j\nu\sigma}$) create (annihilate) holes with orbital μ (ν) and spin σ . $n_{i\mu\sigma}$ is the corresponding number operator. U_μ is the Hubbard type Coulomb repulsion for orbital $\mu = d, p$. ϵ_μ is the orbital on-site energy, and $t_{i\mu j\nu}$ is the tunneling matrix element between $i\mu$ and $j\nu$. Fig. 2 (a) shows the dominant hopping parameters in the CuO_2 plane, where t_{pd} and t_{pp} are the nearest neighbour Cu-O, and O-O hoppings, respectively. The parameters in the hole picture are obtained as $\epsilon_d = 0$ eV, $\epsilon_p = 2.2$ eV, $t_{pd} = 1.3$ eV, and $t_{pp} = 0.6$ eV for La_2CuO_4 from projective Wannier functions [39] applied to non-relativistic full potential local orbital (FPLO) calculations [40][41]. Considering the electronic structure of copper oxides, at charge neutrality the three orbital unit cell includes five electrons and one hole per unit cell such that the d -electron band is half filled. Hole doping is quantified by δ , e.g. 4.5 (4) electrons or 1.5 (2) holes per unit cell means $\delta = 0.5$ (1).

III. AM DRIVEN BY REPULSION ON OXYGEN U_p

In general, the presence of AM in the cuprate planes requires a magnetic moment on the oxygen, thus, not full but only partial occupation, and a finite Hubbard repulsion U_p . It naturally appears in the negative charge transfer limit $\epsilon_p < 0$ at half-filling, when the oxygen orbitals are above the Cu d -orbitals and their partial occupation then enables oxygen AFM once a small Hubbard repulsion U_p is present. Consequently (0, 0)-AM sets in.

Interestingly, altermagnetism can also become stable in the far more realistic *positive* charge transfer regime $\epsilon_p > 0$. It has been shown that already for a low but still realistic charge transfer energy of $\epsilon_p = 2.2$ eV [42]

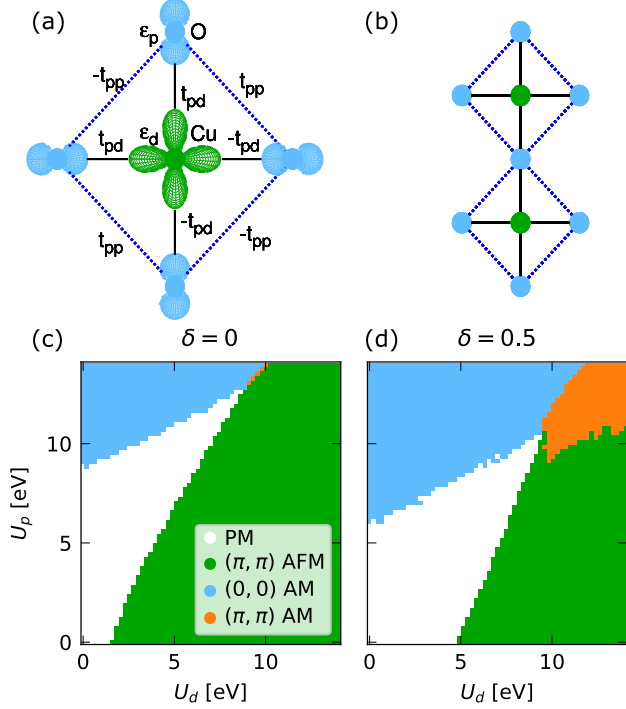


FIG. 2. Illustration of the hopping paths of the three-orbital Emery model (a), and the cluster considered in ED (b). MFT phase diagram for undoped (c) and hole doped (d) case as a function of the Cu and O interaction strengths U_d and U_p . Hole doping is crucial to obtain a (π, π) -AM. It also reduces the critical interaction for the formation of moments on the O atoms, i.e. the $(0,0)$ -AM. [$t_{pd} = 1.3$ eV, $t_{pp} = 0.6$ eV, $\epsilon_p = 2.2$ eV, order parameter threshold 10^{-2} , tol 10^{-5} using a solver (see main text)].

the magnetic moment calculated for the Emery model at half-filling has a 37% contribution from oxygen electrons [8]. This nonzero occupancy can be further enhanced by lowering ϵ_p or by increasing hole doping δ (see below). Naturally, a finite occupancy of oxygen orbitals only triggers AM once the Hubbard repulsion U_p is strong enough. Therefore, in the following we explore U_p dependence of the phase diagram of the Emery model in the realistic positive charge transfer limit. To this end, we elucidate U_p -driven oxygen AFM within a standard Hartree-Fock mean-field theory (MFT).

In the MFT we first split the Hamiltonian \mathcal{H} , Eq. (1), into a non-interacting part \mathcal{H}_0 and an interacting part \mathcal{H}_U , such that $\mathcal{H} = \mathcal{H}_0 + \mathcal{H}_U$. The non-interacting Hamiltonian \mathcal{H}_0 can be diagonalized by Fourier transformation, $c_{k\alpha\sigma} = N^{1/2} \sum_i e^{-ikR_{i\alpha}} c_{k\alpha\sigma}$ and $R_{i\alpha}$ is the position of orbital α in the unit cell i . We obtain $\mathcal{H}_0 = \sum_{k,\sigma} (c_{kd\sigma}, c_{kx\sigma}, c_{ky\sigma})^\dagger h_0(k) (c_{kd\sigma}, c_{kx\sigma}, c_{ky\sigma})$ where

$$h_0(k) = \begin{pmatrix} \epsilon_d & 2it_{pd}s_x & -2it_{pd}s_y \\ -2it_{pd}s_x & \epsilon_p & 4t_{pp}s_x s_y \\ 2it_{pd}s_y & 4t_{pp}s_x s_y & \epsilon_p \end{pmatrix} \quad (2)$$

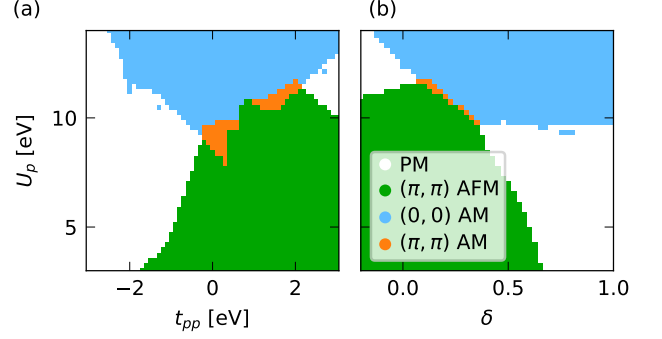


FIG. 3. MFT phase diagram as function of oxygen–oxygen hopping t_{pp} at doping $\delta = 0.5$, panel (a), and as function of hole doping δ at $t_{pp} = 0.6$ eV, panel (b). [$t_{pd} = 1.3$ eV, $\epsilon_p = 2.2$ eV, $U_d = 8$ eV, order parameter threshold 10^{-2} , tol 10^{-5} using a solver (see main text)].

with $s_i = \sin(k_i/2)$. We focus on $(0,0)$ and (π, π) instabilities and introduce two sublattices $\lambda = A, B$ labeling the two copper atoms in the two copper unit cell. We then combine the fermion operators in a twelve-component vector $\Psi_{\mathbf{k}}$ (with indices explicitly written as $\Psi_{\mathbf{k}\alpha\lambda\sigma}$).

We define the mean fields $m_d = \sum_i (-1)^i \langle S_{id}^z \rangle / N$, i.e. the staggered magnetization of the Cu atoms, and $m_p = \sum_i \langle (S_{ix}^z - S_{iy}^z) \rangle / N$, the intra-unit cell staggered magnetization of the p orbitals. Note that by default there are two p orbitals with opposite magnetization in the Wigner–Seitz cell. To complete our ansatz, we also need to account for an interaction-induced change of the relative occupation of the orbitals. By proper renormalization of the chemical potential, it can be incorporated by introducing the third mean field $n_d = \sum_{i,\sigma} \langle c_{id\sigma}^\dagger c_{id\sigma} \rangle / N$ as the filling of the d orbitals in analogy to the overall filling n . Decoupling the Hamiltonian in the charge channel, we find

$$\begin{aligned} \mathcal{H}_U = & \frac{U_d N}{8} (m_d^2 - n_d^2) + \frac{U_p N}{16} (m_d^2 - (n - n_d)^2) \\ & + \sum_{k,\lambda,\sigma} \frac{U_d}{4} (n_d - (-1)^{\lambda+\sigma} m_d) c_{kd\lambda\sigma}^\dagger c_{kd\lambda\sigma} \\ & - \frac{U_p}{8} (-1)^\sigma m_p (c_{kx\lambda\sigma}^\dagger c_{kx\lambda\sigma} - c_{ky\lambda\sigma}^\dagger c_{ky\lambda\sigma}). \quad (3) \end{aligned}$$

The resulting mean-field Hamiltonian $\sum_{\mathbf{k}} \Psi_{\mathbf{k}}^\dagger h(\mathbf{k}) \Psi_{\mathbf{k}} + E_0$ see Appendix Eq. (A4), is a non-interacting Hamiltonian. The 12×12 Bloch Hamiltonian $h(\mathbf{k})$ can be efficiently diagonalized for each momentum to obtain the eigenenergies $\epsilon_m(\mathbf{k})$ and the Bloch eigenstates $|u_m(\mathbf{k})\rangle$ with band index m . Note that H is block-diagonal in spin, but in contrast to the conventional AFM spin density mean-field solution [43] the two blocks are explicitly spin-dependent. We have solved the mean-field equations self-consistently for fixed filling n , i.e. for $\mathcal{M} = (m_d, m_p, n_d, \mu)$ we calculated \mathcal{M}_i from $H(\mathcal{M}_{i-1})$

until $i = 100$, and then applied a python in-build solver which solves the fixpoint equation self-consistently.

The resultant MFT results are displayed in Fig. 2 and Fig. 3 where we find wide regions with both types of AM states. The effect of different parameters is summarized in Tab. I. First, we observe that the key driving term is the interaction U_p on the oxygen orbital, which in conjunction with a direct hopping t_{pp} generates a strong antiferromagnetic exchange between the oxygen moments. However, in order to avoid a full occupation of the p -orbitals, non-zero doping is required or a raise of the on-site energies ϵ_p . At zero doping the single hole is always located entirely on the d -orbital or entirely on the p -orbital, no (π, π) -AM forms. Finite hole doping allows to distribute the additional hole charge between the otherwise competing orbitals which becomes visible by the formation of a (π, π) -AM state, at an increasing critical U_d , and a decreasing critical U_p . Hole doping therefore strengthens the AM phases and weakens the AFM phase, see Fig. 3 (b).

The fact that oxygen and copper are competing for hole charge in order to form a magnetic moment is also evidenced by the observation that the critical U_d for AFM increases when U_p is increased and vice versa, the critical U_p for $(0,0)$ -AM increases when U_d is increased.

Beyond a basic direct exchange picture, the dependence on t_{pp} indicates the importance of a copper-mediated oxygen-oxygen superexchange. The MFT results, see Fig. 3 (a), show that oxygen moments form even for $t_{pp} = 0$ and the lowest critical U_p is found for small positive t_{pp} . Note that the asymmetry in the phase diagram under sign changes of t_{pp} reflects the increased contribution of the p -orbital bands at the Fermi energy.

IV. AM DRIVEN BY OXYGEN-OXYGEN HOPPING t_{pp}

While the MFT has shown that AM states can be stabilized, we next explore the phase diagram within exact diagonalisation (ED) calculations. We confirmed the U_p -driven AM observed in MFT, but interestingly find another route to intra-unit cell oxygen AFM that does not depend on U_p . Instead, it can be triggered by oxygen-oxygen hopping t_{pp} . As this subtle effect depends on the nature of the correlated many-body wave function, it appears in ED but not simple MFT and can be accounted for within cell perturbation theory.

Using the three-orbital Emery model Hamiltonian [Eq. (1)] we performed ED for a cluster of two Cu and seven O at zero doping, i.e., 2 holes in total, shown in Fig. 2 (b). We used $U_d = 8$ eV and $U_p = 4$ eV. We note that for our small ED cluster the resulting ground states do not exhibit a finite magnetization since they cannot spontaneously break symmetries. Instead, we characterize the phases by measuring the spin-spin correlations $\langle \mathbf{S}_i \cdot \mathbf{S}_j \rangle$ for the nearest neighbour Cu-Cu and O-O sites (see Appendix) to diagnose the (π, π) -AFM, $(0,0)$ -AM,

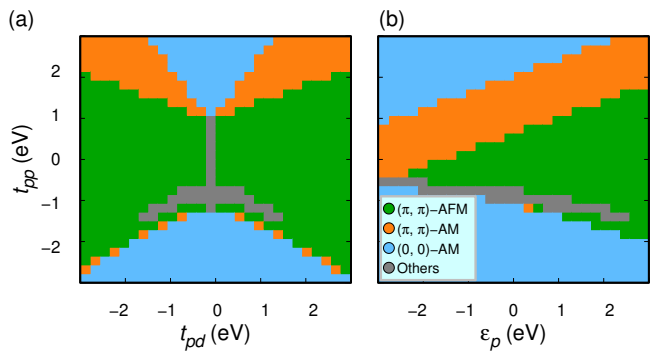


FIG. 4. Phase diagram from exact diagonalization with $U_d = 8$ eV, $U_p = 4$ eV for (a) t_{pd} and t_{pp} ($\epsilon_p = 2.2$ eV) as well as (b) ϵ_p and t_{pp} ($t_{pd} = 1.3$ eV).

and (π, π) -AM states shown in Fig. 1. If spin correlations are incompatible with our ansatzes, phases are labeled as *others*.

The obtained phase diagram is displayed in Fig. 4 (a) for t_{pd} and t_{pp} ($\epsilon_p = 2.2$ eV) as well as (b) ϵ_p and t_{pp} ($t_{pd} = 1.3$ eV). The results differ in two key aspects from the MFT results. First, we can identify t_{pp} as the main driving term of AM, see Fig. 4 (a). Second, and in strong contrast to the MFT result, the formation of oxygen moments depends only weakly on U_p . It points towards a different mechanism driven by the hopping t_{pp} instead of the interaction U_p , which we discuss below.

The sign of t_{pd} does not affect the phase diagram while ϵ_p and t_{pp} are essential. When the magnitude of t_{pp} is small, the phase is a (π, π) -AFM, while increasing t_{pp} can enhance AFM correlations between oxygens and reduce them between coppers, leading to the transition to (π, π) -AM, and then to $(0,0)$ -AM. When t_{pp} is fixed, smaller ϵ_p increases the hole contribution of oxygen, inducing AM correlations.

The main result obtained by ED is that in the limit of realistic charge transfer energy ϵ_p , oxygen-copper hopping t_{pd} , and oxygen repulsion U_p , AFM correlations between oxygens already appear at half-filling, i.e. one hole per CuO_2 unit cell, for only slightly enhanced values of t_{pp} . Moreover, in this regime oxygen magnetism is independent of the value of the oxygen repulsion U_p – instead it is triggered by the oxygen-oxygen hopping t_{pp} .

In table I we summarize the parameter regimes supporting AFM correlations on the oxygens (and therefore AM correlations) obtained from our ED calculations compared to MFT.

The ED findings that AFM correlations can strongly depend on t_{pp} but only weakly on U_p are rather counterintuitive. In the following we provide a qualitative picture motivated by a cell perturbation theory [8]. Following Ref. [8] we can rewrite the charge transfer model Eq.(1) in a different oxygen basis. We define the bonding and antibonding combinations of the four nearest neighbor oxygen orbitals (labeled by L, R, T, B) surrounding the copper d orbital and obtain $|\alpha\rangle \equiv (|p_{xR}\rangle - |p_{yT}\rangle -$

TABLE I. Summary of the parameter regimes supporting AFM correlations on the oxygens as obtained from ED compared to MFT.

| | MFT | ED |
|--------------|-----------------------------------|--------------------------|
| t_{pp} | ≈ 0 or small but positive | $ t_{pp} $ large |
| U_d | small | weak dependence |
| U_p | large U_p crucial | weak dependence on U_p |
| δ | $\delta > 0$ crucial | $\delta > 0$ |
| ϵ_p | small | small |

$(|p_{xL}\rangle + |p_{yB}\rangle)/2$ and $|\beta\rangle \equiv (|p_{xR}\rangle + |p_{yT}\rangle - |p_{xL}\rangle - |p_{yB}\rangle)/2$. Interestingly, we can discard the oxygen repulsion U_p completely such that the Hamiltonian takes the form

$$\begin{aligned}
 \mathcal{H} = & \epsilon_p \sum_{i,\sigma} (\alpha_{i\sigma}^\dagger \alpha_{i,\sigma} + \beta_{i\sigma}^\dagger \beta_{i\sigma}) + 2t_{pd} \sum_{i,j(i),\sigma} \mu(j) c_{id\sigma}^\dagger \alpha_{j\sigma} \\
 & + 2t_{pp} \sum_{i,j(i),\sigma} \nu(j) (\alpha_{i\sigma}^\dagger \alpha_{j\sigma} - \beta_{i\sigma}^\dagger \beta_{j\sigma}) \\
 & + 2t_{pp} \sum_{i,j(i),\sigma} \chi(j) \alpha_{i\sigma}^\dagger \beta_{j\sigma} + \sum_i U n_{i\uparrow} n_{i\downarrow}, \quad (4)
 \end{aligned}$$

where $\alpha_{i,\sigma}^\dagger$ and $\beta_{i,\sigma}^\dagger$ create holes in orthogonalised orbitals α and β centered around copper site i and $\mu(j), \nu(j), \chi(j)$ are the orthogonalisation factors that strongly depend on the distance to j . The crucial point is that the hybridization strength $\chi(j)$ does not have an on-site component but only couples nearest-neighbor orbitals α and β , see Table 1 in Ref. [8].

In most treatments of the charge transfer model Eq.(4) the β orbitals are neglected leading to a two-band model. This, *inter alia*, gives rise to the well-studied antiferromagnetic superexchange processes and the Zhang-Rice singlets upon doping the cuprates [7]. However, our key observation is that neglecting the β orbitals is no longer justified once $|t_{pp}|$ is larger than assumed in most cuprate works and once the β orbital is not fully occupied. It is the nearest neighbor hybridization between oxygen orbitals that induces oxygen AFM.

Then a simple picture emerges best explained in a minimal toy-model. From Eq.(4) we concentrate on two plaquettes (one of each A and B sublattices) and two holes. First, for infinite Coulomb repulsion on the copper d orbital strong super exchange leads to copper AFM [8], e.g. plaquette A spin up in the d orbital and plaquette B spin down. Next, the standard local hybridization between d and α orbitals leads to AFM correlations between plaquettes admixing oxygen states to the magnetic moment [8]. Going beyond this picture, we take into account the nearest neighbor α, β hybridisation. An up spin in α orbitals of site A induces an up spin in β orbitals at site B and vice versa. As a result, the spin of bonding/antibonding oxygen orbitals is anti-aligned in each plaquette (thus aligned between neighboring plaquettes). The hybridisation between the nearest neighbor α, β orbitals is directly

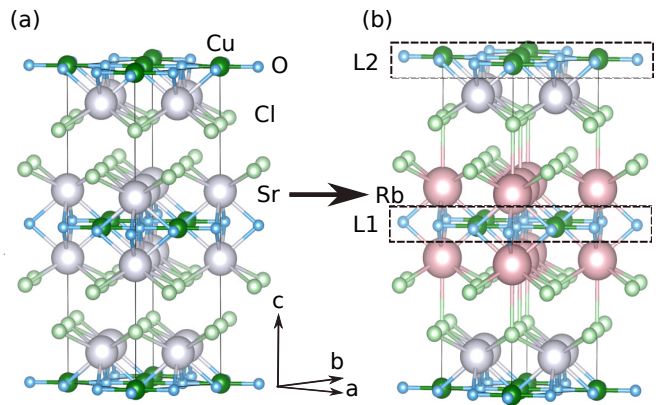


FIG. 5. Crystal structure of (a) $\text{Sr}_2\text{CuO}_2\text{Cl}_2$ and (b) $\text{SrRbCuO}_2\text{Cl}_2$. L1 and L2 label two CuO_2 layers.

proportional to t_{pp} and when calculating spin correlations in this state between the original oxygen ligands in the unit cell they are indeed AFM.

V. AM DRIVEN BY LARGE DOPING IN A MATERIAL CANDIDATE

Finding large values of U_p and t_{pp} in cuprate materials is not simple but we scanned different candidates for AM using *ab initio* density functional theory based calculations. The first candidate is the widely studied cuprate La_2CuO_4 , where it is difficult to obtain in-plane oxygen moments since the extra holes from doping prefer to stay in apices O locations. We therefore turn our attention to the compound $\text{Sr}_2\text{CuO}_2\text{Cl}_2$ [44], where the out-of-plane oxygen ions at the apices of the CuO_6 octahedra are replaced by Cl. In addition, smaller ϵ_p has also been proposed, *cf.* [45] and Table I available in its arXiv version [46].

In Fig. 5 (a) we show the tetragonal structure of $\text{Sr}_2\text{CuO}_2\text{Cl}_2$ with space group $I4/mmm$. Unlike La_2CuO_4 , no long-range tilting/rotation of the CuO_4Cl_2 octahedra is present. The structure leads to a very small magnetic anisotropy [47–50] and very weak interlayer coupling [50], making $\text{Sr}_2\text{CuO}_2\text{Cl}_2$ a better two-dimensional AFM insulator [50–52]. Both, inelastic neutron and light scattering measurements found a high-energy continuum of magnetic fluctuations [53] and multiple-magnon excitations [54]. Similar to La_2CuO_4 , the valence of the Cu atoms is +2, with one hole per copper atom. In order to have oxygen magnetic moments, we replaced half of the Sr atoms by Rb so that the system $\text{SrRbCuO}_2\text{Cl}_2$ [See Fig. 5 (b)] is hole doped, and becomes metallic. The CuO_4 layer neighbor to Rb (Sr) is labeled as L1 (L2). The structure was fully relaxed with GGA using the Vienna *ab initio* simulation package (VASP) [55, 56]. Total energies for various spin configurations and corresponding band structures were calculated with GGA+ U . We considered contributions of the

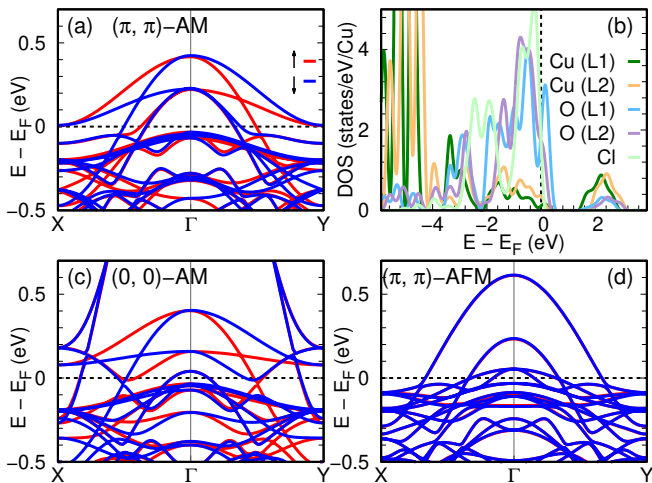


FIG. 6. (a) Band structure and (b) density of states for SrRbCuO₂Cl₂ in the (π, π) -AM magnetic order within GGA+ U from DFT as shown in Fig. 1. Band structure in the (c) $(0, 0)$ -AM magnetic order and (d) (π, π) -AFM order are also shown. Colors red (spin \uparrow) and blue (spin \downarrow) indicate the up bands and down states, respectively. The altermagnetic ordering is clear from the spin splitting along Γ -X and Γ -Y.

Coulomb repulsion [57], $U_{\text{eff}} = U - J_H = 8$ eV for Cu following [58] within GGA+ U , and adopted a cutoff energy of 520 eV and Monkhorst-pack k -points generated with $12 \times 12 \times 4$.

By comparing the energy for various magnetic configurations; Cu AFM order, (π, π) -AM order, and $(0, 0)$ -AM order, we find that (π, π) -AM order is 241.5 meV lower than $(0, 0)$ -AM and 53.9 meV lower than (π, π) -AFM. The magnetic moments are $0.6 \mu_B$ for Cu, similar to La₂CuO₄ [38]. However, in contrast to La₂CuO₄, which has a small oxygen moment on the apical oxygen [38] but no doping-induced oxygen magnetism in the CuO₂ plane, in SrRbCuO₂Cl₂ the magnetic moments are $0.4 \mu_B$ for oxygen. We integrated the partial density of states for Cu and O and find that the additional four holes from doping are mostly localized at the four O in the L1 layer shown in Fig. 6 (b) with doping $\delta = -2$ (3 electrons, 3 holes per CuO₂).

The resulting band structure within GGA+ U ($U_d = 8$ eV, $U_p = 0$ eV) obtained from DFT is displayed in Fig. 6 for (π, π) -AM order, $(0, 0)$ -AM order, and (π, π) -AFM order. The bands have opposite spin-splitting sign along Γ -X and Γ -Y. We stress that, different from the case of La₂CuO₄, where AM originates from CuO₆ octahedra distortions, in SrRbCuO₂Cl₂ such distortions are absent and AM arises from oxygen moments.

VI. CONCLUSION

We have studied d -wave magnetism in cuprates induced by magnetic moments on the oxygen atoms. Fo-

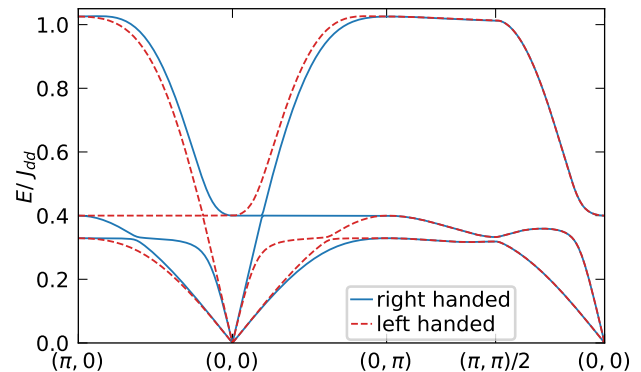


FIG. 7. Magnon spectrum along a high symmetry path through the magnetic Brillouin zone, determined from linear spin wave theory of an effective Heisenberg-like spin only model with moments on the oxygens and copper atoms for the (π, π) -AM state, see Eq. (C1) in the supplementary material. The different chiralities (left and right precessing) are distinguished by color and linestyle. Note, we have used an artificially large splitting for presentation. [$J_{pd} = 0.5J_{dd}$ and $J_{pp} = 0.4J_{dd}$]

cusing on the three-orbital Emery model we employed Hartree-Fock MFT, exact diagonalization of finite clusters, and cell perturbation theory to uncover distinct mechanisms stabilizing AFM correlations between oxygen moments. Two different AM states can be stabilized. First, a $(0, 0)$ -AM with AFM ordered moments only on the oxygen sites, such that the magnetic unit cell is identical with the crystal unit cell. The Fermi surface is characterized by a large spin splitting of the formerly (π, π) centered pocket into open Fermi surfaces along the crystallographic axis, see Fig. 1. Interestingly, this intra-unit cell magnetic order has been proposed previously to explain inelastic neutron scattering data [16, 17]. Secondly, we find a (π, π) -AM with AFM order of the oxygens as above coexisting with the standard (π, π) magnetic order on the copper atoms. Here, we observe a Fermi surface with two closed pockets which are additionally weakly spin split by opposite tilting, see Fig. 1.

Our work shows that AM states in cuprates can be stabilized in ED, MFT, DFT and cell perturbation theory. The exact form of the phase boundaries is method dependent. Based on our observations, we identify three distinct mechanisms driving AM in cuprates: (i) a direct exchange between the oxygens requiring a large oxygen interaction U_p , (ii) strong charge transfer, i.e., ϵ_p small, bringing the p -oxygen orbital closer to the Fermi energy, and (iii) a large oxygen-oxygen hopping t_{pp} effectively such that the magnetic order of the copper atoms induces magnetic order on oxygen sites. Beyond our proof of principle calculations on the minimal Emery model, we also investigated the realization of AM in a novel candidate material SrRbCuO₂Cl₂ based on the well-known existing system Sr₂CuO₂Cl₂. The DFT results suggest the (π, π) -AM order to be the most stable one emerging

from AFM correlations between oxygen moments.

The prospect of AM in doped cuprates raises the question on how it would manifest in experiments. Apart from the standard spin transport signatures predicted for AM [24, 25, 59], angle resolved photoemission spectroscopy (ARPES) or spin ARPES [60] could directly probe the spin splitting of the Fermi surface. Alternatively, the split FS can be detected by quantum oscillation measurements which have a long history in underdoped cuprates [61, 62]. Interestingly, since Zeeman coupling will lead to different areas for the spin-polarized FSs, the temperature dependence of QO can be unconventional [63, 64] and new low frequency oscillations could appear [65, 66].

Most promising would be to revisit previous inelastic neutron scattering experiments [16, 17]. Magnon spectra of AM display chirality split magnons away from high symmetry points. The splitting is potentially small and requires high resolution. In Fig. 7 we show predictions for magnon spectra with chirality split magnon bands. Note, we treated a simple Heisenberg like model of spins on copper and oxygen sites, see Appendix for details, and the optical magnon modes from intra-unit cell excitations are strongly split, but because of the weak oxygen moment might be hard to observe.

Finally, AM in cuprates or other related compounds would have important ramifications for superconductivity. AM have been shown to lead to unconventional phenomena [67–71] such as pair density states (PDW) with finite momentum pairing [72–75]. Especially the (0, 0)-AM offers – due to its large spin-splitting and absence of magnetism for the copper sites – an interesting platform for realizing PDWs. Searching for signatures thereof in experiment and understanding the microscopic mechanism for its realization in realistic settings will be important directions for future research.

Note added. Upon completion of this work, we became aware of an independent work by Dürrnagel et al. [76] which explored an itinerant AM phase transition emanating from an electronic model on a related Lieb lattice, where AM originates from sublattice interference of the enlarged unit cell.

ACKNOWLEDGMENTS

We thank Mark Fisher, Kemp Plumb, Alexander Mook and Igor I. Mazin for insightful discussions. Y. L. acknowledges support from the Alexander von Humboldt Foundation through a postdoctoral Humboldt fellowship and National Natural Science Foundation of China (Grant No. 12004296). V. L. acknowledges support from the Studienstiftung des deutschen Volkes. J. K. acknowledges support from the Imperial-TUM flagship partnership. R.V. acknowledges support by the Deutsche Forschungsgemeinschaft (DFG, German Research Foundation) for funding through Project No. TRR 288 — 422213477 (project A05, B05) and Project No. VA

117/23-1 — 509751747. Collaboration between J.K. and K.W. was supported by the ‘Tandems for Excellence: Visiting Researchers Programme’ of the University of Warsaw.

Appendix A: Mean-field theory

The 12×12 Hamiltonian is block-diagonal in spin. We consider the ordered basis

$$\psi_{\mathbf{k}} = (c_{\mathbf{k}dA\uparrow}, c_{\mathbf{k}xA\uparrow}, c_{\mathbf{k}yA\uparrow}, c_{\mathbf{k}dB\uparrow}, c_{\mathbf{k}xB\uparrow}, c_{\mathbf{k}yB\uparrow}, c_{\mathbf{k}dA\downarrow}, c_{\mathbf{k}xA\downarrow}, c_{\mathbf{k}yA\downarrow}, c_{\mathbf{k}dB\downarrow}, c_{\mathbf{k}xB\downarrow}, c_{\mathbf{k}yB\downarrow})^T. \quad (\text{A1})$$

The matrix elements are

$$\begin{aligned} h(\mathbf{k}) = & \mathbb{1} \otimes \begin{pmatrix} h_{AA}(\mathbf{k}) & h_{AB}(\mathbf{k}) \\ h_{AB}(\mathbf{k})^\dagger & h_{AA}(\mathbf{k}) \end{pmatrix} \\ & - \frac{U_d m_d}{4} \tau^z \otimes \tau^z \otimes \begin{pmatrix} 1 & 0 & 0 \\ 0 & 0 & 0 \\ 0 & 0 & 0 \end{pmatrix} \\ & + \frac{U_d n_d}{4} \mathbb{1} \otimes \mathbb{1} \otimes \begin{pmatrix} 1 & 0 & 0 \\ 0 & 0 & 0 \\ 0 & 0 & 0 \end{pmatrix} \\ & - \frac{U_p m_p}{8} \tau^z \otimes \mathbb{1} \otimes \begin{pmatrix} 0 & 0 & 0 \\ 0 & 1 & 0 \\ 0 & 0 & -1 \end{pmatrix} \\ & + \frac{U_p (n - n_d)}{8} \mathbb{1} \otimes \mathbb{1} \otimes \begin{pmatrix} 0 & 0 & 0 \\ 0 & 1 & 0 \\ 0 & 0 & 1 \end{pmatrix} \quad (\text{A2}) \end{aligned}$$

$$h_{AA}(\mathbf{k}) = \begin{pmatrix} 0 & -t_{pd}e^{-ik_x/2} & t_{pd}e^{-ik_y/2} \\ -t_{pd}e^{ik_x/2} & 0 & 2t_{pp} \cos\left(\frac{k_x - k_y}{2}\right) \\ t_{pd}e^{ik_y/2} & 2t_{pp} \cos\left(\frac{k_x - k_y}{2}\right) & 0 \end{pmatrix} \quad (\text{A3})$$

$$h_{AB}(\mathbf{k}) = \begin{pmatrix} 0 & t_{pd}e^{-ik_x/2} & -t_{pd}e^{-ik_y/2} \\ t_{pd}e^{ik_x/2} & 0 & -2t_{pp} \cos\left(\frac{k_x + k_y}{2}\right) \\ -t_{pd}e^{ik_y/2} & -2t_{pp} \cos\left(\frac{k_x + k_y}{2}\right) & 0 \end{pmatrix} \quad (\text{A4})$$

and τ^z is the Pauli- z matrix.

Appendix B: Spin-Spin correlations from ED

Fig. 8 display the spin-spin correlations for exact diagonalization of two-copper-sites cluster using $U_d = 8$ eV, $U_p = 4$ eV.

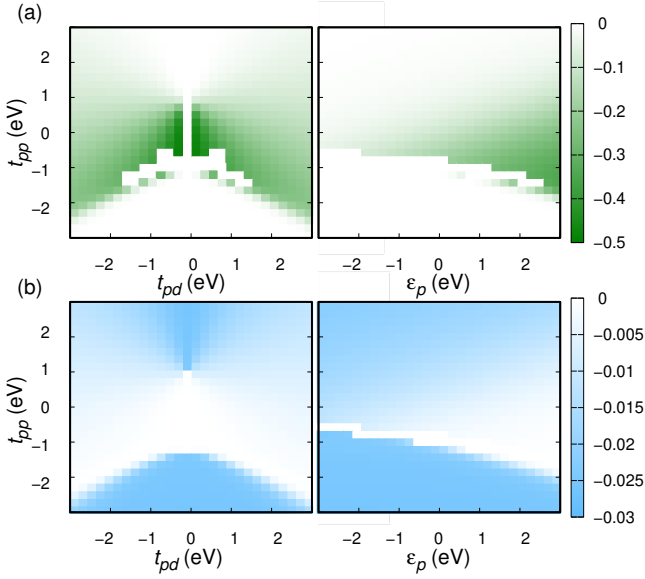


FIG. 8. Spin-spin correlations with respect to t_{pd} and t_{pp} ($\epsilon_p = 2.2$ eV) as well as ϵ_p and t_{pp} ($t_{pd} = 1.3$ eV). (a) nearest neighbour Cu-Cu correlation ($\langle S_i^d S_j^d \rangle$) (b) nearest neighbour O-O correlations ($\langle S_i^p S_j^p \rangle$).

Appendix C: Magnon spectrum

1. Model

We study the effective Heisenberg-like spin-only model

$$\begin{aligned} H_{\text{spin}} &= \sum_{\langle ij \rangle} J_{\alpha\beta} \mathbf{S}_{i\alpha} \mathbf{S}_{j\beta} \\ &= \sum_{\langle ij \rangle} J_{\alpha\beta} \left(S_{i\alpha}^z S_{j\beta}^z + \frac{1}{2} S_{i\alpha}^+ S_{j\beta}^- + \frac{1}{2} S_{i\alpha}^- S_{j\beta}^+ \right) \end{aligned} \quad (\text{C1})$$

which emerges in the large U limit from eq. (1) of the main text. It includes AFM exchange $J_{dd} > 0$ between the spin-1/2 located at the positions of the Cu atoms, AFM exchange $J_{pp} > 0$ between the spin-1/2 located at the positions of the O atoms and a interaction J_{pd} between O and Cu moments. $S_{i\alpha}^\nu$ are the spin-1/2 operators and $S_{i\alpha}^\pm$ the raising and lowering operators.

2. Linear spin-wave theory

We evaluate the magnon spectrum assuming the ordered groundstate of the (π, π) -AM, shown in Fig. 1 of the main text. We introduce 2 sublattices λ , employ a Holstein-Primakoff transformation, and take the large S limit. If the spin at i, α, λ is \uparrow the transformation reads

$$\begin{aligned} S_{i\alpha\lambda}^z &= S_\alpha - a_{i\alpha\lambda}^\dagger a_{i\alpha\lambda} \\ S_{i\alpha\lambda}^+ &= \sqrt{2S_\alpha} a_{i\alpha\lambda}^\dagger \\ S_{i\alpha\lambda}^- &= \sqrt{2S_\alpha} a_{i\alpha\lambda} \end{aligned} \quad (\text{C2})$$

and

$$\begin{aligned} S_{i\alpha\lambda}^z &= -S_\alpha + a_{i\alpha\lambda}^\dagger a_{i\alpha\lambda} \\ S_{i\alpha\lambda}^+ &= \sqrt{2S_\alpha} a_{i\alpha\lambda}^\dagger \\ S_{i\alpha\lambda}^- &= \sqrt{2S_\alpha} a_{i\alpha\lambda} \end{aligned} \quad (\text{C3})$$

for a \downarrow spin. The operator $a_{i\alpha\lambda}$ ($a_{i\alpha\lambda}^\dagger$) annihilates (creates) a magnon, i.e. a spin flip, at i, α, λ .

Keeping only terms linear or quadratic in S_α

$$\begin{aligned} H_{\text{spin}} &= -4J_{dd}S_d^2 - 8J_{pp}S_p^2 + \\ &+ \sum_{\mathbf{k}} \boldsymbol{\eta}_{\mathbf{k}L}^\dagger h_L(\mathbf{k}) \boldsymbol{\eta}_{\mathbf{k}L} + \boldsymbol{\eta}_{\mathbf{k}R}^\dagger h_R(\mathbf{k}) \boldsymbol{\eta}_{\mathbf{k}R} + \mathcal{O}(S_\alpha^0) \end{aligned} \quad (\text{C4})$$

which simplifies for $S_\alpha = 1/2$ to

$$H_{\text{spin}} = -J_{dd} - 2J_{pp} + \sum_{\mathbf{k}} \boldsymbol{\eta}_{\mathbf{k}L}^\dagger h_L(\mathbf{k}) \boldsymbol{\eta}_{\mathbf{k}L} + \boldsymbol{\eta}_{\mathbf{k}R}^\dagger h_R(\mathbf{k}) \boldsymbol{\eta}_{\mathbf{k}R}. \quad (\text{C5})$$

We defined $a_{\mathbf{k}\alpha\lambda}^\dagger = N^{-1/2} \sum_j e^{i\mathbf{k}\mathbf{R}_{j\alpha\lambda}} a_{j\alpha\lambda}^\dagger$ where $\mathbf{R}_{j\alpha\lambda}$ is the position of a site j, α, λ and the fields

$$\boldsymbol{\eta}_{\mathbf{k}R} = (a_{\mathbf{k}dA}, a_{\mathbf{k}xA}, a_{\mathbf{k}xB}, a_{-\mathbf{k}dB}^\dagger, a_{-\mathbf{k}yA}^\dagger, a_{-\mathbf{k}yB}^\dagger) \quad (\text{C6})$$

$$\boldsymbol{\eta}_{\mathbf{k}L} = (a_{\mathbf{k}dB}, a_{\mathbf{k}yA}, a_{\mathbf{k}yB}, a_{-\mathbf{k}dA}^\dagger, a_{-\mathbf{k}xA}^\dagger, a_{-\mathbf{k}xB}^\dagger). \quad (\text{C7})$$

The matrix elements are given by

$$\begin{aligned} h_R(\mathbf{k}) &= \begin{pmatrix} h_{pd}(k_x) & h_{pd}(k_y) + h_0(\mathbf{k}) \\ h_{pd}^\dagger(k_y) + h_0(\mathbf{k}) & h_{pd}(-k_y) \end{pmatrix} \\ &+ (J_{dd}, J_{pp}, J_{pp}, J_{dd}, J_{pp}, J_{pp}) \mathbb{1} \end{aligned} \quad (\text{C8})$$

$$\begin{aligned} h_0(\mathbf{k}) &= \\ &\begin{pmatrix} \frac{J_{dd}}{2} (\cos k_x + \cos k_y) & 0 & 0 \\ 0 & \frac{J_{pp}}{2} \cos \frac{k_x - k_y}{2} & \frac{J_{pp}}{2} \cos \frac{k_x + k_y}{2} \\ 0 & \frac{J_{pp}}{2} \cos \frac{k_x + k_y}{2} & \frac{J_{pp}}{2} \cos \frac{k_x - k_y}{2} \end{pmatrix} \end{aligned} \quad (\text{C9})$$

$$h_{pd}(k) = \frac{J_{pd}}{4} \begin{pmatrix} 0 & e^{ik/2} & e^{-ik/2} \\ e^{-ik/2} & 0 & 0 \\ e^{ik/2} & 0 & 0 \end{pmatrix} \quad (\text{C10})$$

and $h_L((k_x, k_y)) = h_R((-k_y, -k_x))$. Note however that $h_0((k_x, k_y)) = h_0((-k_y, -k_x))$ such that the matrices differ only in terms which are proportional to J_{pd} .

We diagonalize (C5) by a numerical Bogoliubov transformation, i.e. we multiply $h_{R,L}$ with the matrix $\mathbb{1}(1, 1, 1, -1, -1, -1)$ and then diagonalize this non-hermitian matrix. The positive eigenvalues yield the magnon spectrum of (C1).

3. Results

The resulting magnon spectrum, see Fig. 7, features two Goldstone modes, a flat mode which can be associated with the ordering of the oxygen moments and a

steep mode from the copper moments, because $J_{dd} > J_{pp}$. Additionally, an optical mode with oxygen orbital character appears due to the fact that the AFM ordering of the oxygen moments is intra unit cell. We observe large chirality splitting of the magnon modes because we

expect $J_{pd} > J_{pp}$. We expect that most of the spectral weight is located on the magnon branches with Cu orbital character. However, quantitative studies of the dynamic spin structure factor of more microscopic model remains a formidable task for future.

-
- [1] J. G. Bednorz and K. A. Müller, Possible high- T_c superconductivity in the Ba- La- Cu- O system, *Zeitschrift für Physik B Condensed Matter* **64**, 189 (1986).
- [2] P. W. Anderson, The resonating valence bond state in La_2CuO_4 and superconductivity, *Science* **235**, 1196 (1987).
- [3] C. Gros and R. Valentí, A self-consistent cluster study of the emery model, *Annalen der Physik* **506**, 460 (1994).
- [4] E. Dagotto, Correlated electrons in high-temperature superconductors, *Rev. Mod. Phys.* **66**, 763 (1994).
- [5] M. Imada, A. Fujimori, and Y. Tokura, Metal-insulator transitions, *Rev. Mod. Phys.* **70**, 1039 (1998).
- [6] V. Emery, Theory of high- T_c superconductivity in oxides, *Physical Review Letters* **58**, 2794 (1987).
- [7] F. C. Zhang and T. M. Rice, Effective hamiltonian for the superconducting Cu oxides, *Phys. Rev. B* **37**, 3759 (1988).
- [8] J. H. Jefferson, H. Eskes, and L. F. Feiner, Derivation of a single-band model for CuO_2 planes by a cell-perturbation method, *Phys. Rev. B* **45**, 7959 (1992).
- [9] C. Weber, T. Giamarchi, and C. M. Varma, Phase diagram of a three-orbital model for high- T_c cuprate superconductors, *Phys. Rev. Lett.* **112**, 117001 (2014).
- [10] K. Sheshadri, D. Malterre, A. Fujimori, and A. Chainani, Connecting the one-band and three-band hubbard models of cuprates via spectroscopy and scattering experiments, *Phys. Rev. B* **107**, 085125 (2023).
- [11] M. H. Fischer and E.-A. Kim, Mean-field analysis of intra-unit-cell order in the emery model of the CuO_2 plane, *Phys. Rev. B* **84**, 144502 (2011).
- [12] M. H. Fischer, S. Wu, M. Lawler, A. Paramekanti, and E.-A. Kim, Nematic and spin-charge orders driven by hole-doping a charge-transfer insulator, *New Journal of Physics* **16**, 093057 (2014).
- [13] C. Varma, Theory of the pseudogap state of the cuprates, *Physical Review B* **73**, 155113 (2006).
- [14] S. Chakravarty, R. Laughlin, D. K. Morr, and C. Nayak, Hidden order in the cuprates, *Physical Review B* **63**, 094503 (2001).
- [15] A. C. Walters, T. G. Perring, J.-S. Caux, A. T. Savici, G. D. Gu, C.-C. Lee, W. Ku, and I. A. Zaliznyak, Effect of covalent bonding on magnetism and the missing neutron intensity in copper oxide compounds, *Nature Physics* **5**, 867 (2009).
- [16] B. Fauqué, Y. Sidis, V. Hinkov, S. Pailhes, C. Lin, X. Chaud, and P. Bourges, Magnetic order in the pseudogap phase of high- T_c superconductors, *Physical Review Letters* **96**, 197001 (2006).
- [17] Y. Li, V. Balédent, N. Barišić, Y. Cho, B. Fauqué, Y. Sidis, G. Yu, X. Zhao, P. Bourges, and M. Greven, Unusual magnetic order in the pseudogap region of the superconductor $\text{HgBa}_2\text{CuO}_{4+\delta}$, *Nature* **455**, 372 (2008).
- [18] K.-H. Ahn, A. Hariki, K.-W. Lee, and J. Kuneš, Antiferromagnetism in RuO_2 as d-wave pomeranchuk instability, *Physical Review B* **99**, 184432 (2019).
- [19] S. Hayami, Y. Yanagi, and H. Kusunose, Momentum-dependent spin splitting by collinear antiferromagnetic ordering, *Journal of the Physical Society of Japan* **88**, 123702 (2019).
- [20] L. Šmejkal, R. González-Hernández, T. Jungwirth, and J. Sinova, Crystal time-reversal symmetry breaking and spontaneous hall effect in collinear antiferromagnets, *Science Advances* **6**, eaaz8809 (2020).
- [21] L.-D. Yuan, Z. Wang, J.-W. Luo, E. I. Rashba, and A. Zunger, Giant momentum-dependent spin splitting in centrosymmetric low- z antiferromagnets, *Phys. Rev. B* **102**, 014422 (2020).
- [22] H.-Y. Ma, M. Hu, N. Li, J. Liu, W. Yao, J.-F. Jia, and J. Liu, Multifunctional antiferromagnetic materials with giant piezomagnetism and noncollinear spin current, *Nature Communications* **12**, 2846 (2021).
- [23] I. I. Mazin, K. Koepernik, M. D. Johannes, R. González-Hernández, and L. Šmejkal, Prediction of unconventional magnetism in doped FeSb_2 , *Proceedings of the National Academy of Sciences* **118**, e2108924118 (2021).
- [24] L. Šmejkal, J. Sinova, and T. Jungwirth, Emerging research landscape of altermagnetism, *Phys. Rev. X* **12**, 040501 (2022).
- [25] L. Šmejkal, J. Sinova, and T. Jungwirth, Beyond conventional ferromagnetism and antiferromagnetism: A phase with nonrelativistic spin and crystal rotation symmetry, *Phys. Rev. X* **12**, 031042 (2022).
- [26] L. Šmejkal, A. B. Hellenes, R. González-Hernández, J. Sinova, and T. Jungwirth, Giant and tunneling magnetoresistance in unconventional collinear antiferromagnets with nonrelativistic spin-momentum coupling, *Phys. Rev. X* **12**, 011028 (2022).
- [27] V. Leeb, A. Mook, L. Šmejkal, and J. Knolle, Spontaneous formation of altermagnetism from orbital ordering, *Physical Review Letters* **132**, 236701 (2024).
- [28] I. Mazin (The PRX Editors), Editorial: Altermagnetism—a new punch line of fundamental magnetism, *Phys. Rev. X* **12**, 040002 (2022).
- [29] H. O. Jeschke, M. Shimizu, and I. I. Mazin, $\text{CuAg}(\text{SO}_4)_2$: A doubly strongly correlated altermagnetic three-dimensional analog of the parent compounds of high- T_c cuprates, *Phys. Rev. B* **109**, L220412 (2024).
- [30] A. Bose, S. Vadnais, and A. Paramekanti, Altermagnetism and superconductivity in a multiorbital t-J model, *arXiv preprint arXiv:2403.17050* (2024).
- [31] S. Giuli, C. Mejuto-Zaera, and M. Capone, Altermagnetism from interaction-driven itinerant magnetism, *arXiv preprint arXiv:2410.00909* (2024).
- [32] J. Zaanen, G. A. Sawatzky, and J. W. Allen, Band gaps and electronic structure of transition-metal compounds, *Phys. Rev. Lett.* **55**, 418 (1985).
- [33] S. Uchida, T. Ido, H. Takagi, T. Arima, Y. Tokura, and S. Tajima, Optical spectra of $\text{La}_{2-x}\text{Sr}_x\text{CuO}_4$: Effect of

- carrier doping on the electronic structure of the CuO_2 plane, *Phys. Rev. B* **43**, 7942 (1991).
- [34] M. T. Czyżyk and G. A. Sawatzky, Local-density functional and on-site correlations: The electronic structure of La_2CuO_4 and LaCuO_3 , *Phys. Rev. B* **49**, 14211 (1994).
- [35] S. Pesant and M. Côté, DFT + U study of magnetic order in doped La_2CuO_4 crystals, *Phys. Rev. B* **84**, 085104 (2011).
- [36] J. W. Furness, Y. Zhang, C. Lane, I. G. Buda, B. Barbiellini, R. S. Markiewicz, A. Bansil, and J. Sun, An accurate first-principles treatment of doping-dependent electronic structure of high-temperature cuprate superconductors, *Communications Physics* **1**, 11 (2018).
- [37] M. Biemann, P. Schwaller, P. Ruffieux, O. Gröning, L. Schlapbach, and P. Gröning, Ago investigated by photoelectron spectroscopy: Evidence for mixed valence, *Phys. Rev. B* **65**, 235431 (2002).
- [38] C. Lane, J. W. Furness, I. G. Buda, Y. Zhang, R. S. Markiewicz, B. Barbiellini, J. Sun, and A. Bansil, Antiferromagnetic ground state of La_2CuO_4 : A parameter-free ab initio description, *Phys. Rev. B* **98**, 125140 (2018).
- [39] H. Eschrig and K. Koepf, Tight-binding models for the iron-based superconductors, *Phys. Rev. B* **80**, 104503 (2009).
- [40] K. Koepf and H. Eschrig, Full-potential nonorthogonal local-orbital minimum-basis band-structure scheme, *Phys. Rev. B* **59**, 1743 (1999).
- [41] We extracted the parameters employing the Perdew-Burke-Ernzerhof generalized gradient approximation (GGA) [77] as exchange-correlation functional and a mesh of $9 \times 9 \times 5$ \mathbf{k} points in the first Brillouin zone (FBZ).
- [42] And for infinitely large copper repulsion U_d and realistic oxygen-oxygen hopping $t_{pp} = 0.6$ eV.
- [43] J. Knolle, I. Eremin, and R. Moessner, Multiorbital spin susceptibility in a magnetically ordered state: Orbital versus excitonic spin density wave scenario, *Physical Review B* **83**, 224503 (2011).
- [44] L. L. Miller, X. L. Wang, S. X. Wang, C. Stassis, D. C. Johnston, J. Faber, and C.-K. Loong, Synthesis, structure, and properties of $\text{Sr}_2\text{CuO}_2\text{Cl}_2$, *Phys. Rev. B* **41**, 1921 (1990).
- [45] C. Weber, C. Yee, K. Haule, and G. Kotliar, Scaling of the transition temperature of hole-doped cuprate superconductors with the charge-transfer energy, *Europhysics Letters* **100**, 37001 (2012).
- [46] C. Weber, C.-H. Yee, K. Haule, and G. Kotliar, Scaling of the transition temperature of hole-doped cuprate superconductors with the charge-transfer energy, *arXiv preprint arXiv:1108.3028* (2011).
- [47] A. Cuccoli, T. Roscilde, R. Vaia, and P. Verrucchi, Detection of xy behavior in weakly anisotropic quantum antiferromagnets on the square lattice, *Phys. Rev. Lett.* **90**, 167205 (2003).
- [48] B. J. Suh, F. Borsa, L. L. Miller, D. C. Johnston, D. R. Torgeson, and M. Corti, Evidence for crossover effects in the spin dynamics of the two-dimensional antiferromagnet $\text{Sr}_2\text{CuO}_2\text{Cl}_2$ from ^{35}Cl nuclear magnetic resonance, *Journal of Applied Physics* **79**, 5084 (1996).
- [49] K. Katsumata, M. Hagiwara, Z. Honda, J. Satooka, A. Aharony, R. J. Birgeneau, F. C. Chou, O. Entin-Wohlman, A. B. Harris, M. A. Kastner, Y. J. Kim, and Y. S. Lee, Direct observation of the quantum energy gap in $s = \frac{1}{2}$ tetragonal cuprate antiferromagnets, *Europhysics Letters* **54**, 508 (2001).
- [50] B. O. Wells, Z. X. Shen, A. Matsuura, D. M. King, M. A. Kastner, M. Greven, and R. J. Birgeneau, E versus k relations and many body effects in the model insulating copper oxide $\text{Sr}_2\text{CuO}_2\text{Cl}_2$, *Phys. Rev. Lett.* **74**, 964 (1995).
- [51] A. N. Yaresko, A. Y. Perlov, R. Hayn, and H. Rosner, Exchange integrals of $\text{Sr}_2\text{CuO}_2\text{Cl}_2$ and $\text{Ba}_2\text{Cu}_3\text{O}_4\text{Cl}_2$ from LDA + U calculations, *Phys. Rev. B* **65**, 115111 (2002).
- [52] A. d. l. Torre, K. L. Seyler, L. Zhao, S. D. Matteo, M. S. Scheurer, Y. Li, B. Yu, M. Greven, S. Sachdev, M. R. Norman, and D. Hsieh, Mirror symmetry breaking in a model insulating cuprate, *Nature Physics* **17**, 777 (2021).
- [53] K. W. Plumb, A. T. Savici, G. E. Granroth, F. C. Chou, and Y.-J. Kim, High-energy continuum of magnetic excitations in the two-dimensional quantum antiferromagnet $\text{Sr}_2\text{CuO}_2\text{Cl}_2$, *Phys. Rev. B* **89**, 180410 (2014).
- [54] D. Betto, R. Fumagalli, L. Martinelli, M. Rossi, R. Pionto, K. Yoshimi, D. Di Castro, E. Di Gennaro, A. Sambri, D. Bonn, G. A. Sawatzky, L. Braicovich, N. B. Brookes, J. Lorenzana, and G. Ghiringhelli, Multiple-magnon excitations shape the spin spectrum of cuprate parent compounds, *Phys. Rev. B* **103**, L140409 (2021).
- [55] G. Kresse and J. Furthmüller, Efficiency of ab-initio total energy calculations for metals and semiconductors using a plane-wave basis set, *Comput. Mater. Sci.* **6**, 15 (1996).
- [56] J. Hafner, *Ab-initio* simulations of materials using vasp: Density-functional theory and beyond, *J. Comput. Chem.* **29**, 2044 (2008).
- [57] S. L. Dudarev, G. A. Botton, S. Y. Savrasov, C. J. Humphreys, and A. P. Sutton, Electron-energy-loss spectra and the structural stability of nickel oxide: An LSDA+U study, *Phys. Rev. B* **57**, 1505 (1998).
- [58] T. C. Sterling and D. Reznik, Effect of the electronic charge gap on lo bond-stretching phonons in undoped La_2CuO_4 calculated using LDA + U, *Phys. Rev. B* **104**, 134311 (2021).
- [59] R. D. Gonzalez Betancourt, J. Zubáč, K. Geishendorf, P. Ritzinger, B. Růžicková, T. Kotte, J. Železný, K. Olejník, G. Springholz, B. Büchner, *et al.*, Anisotropic magnetoresistance in altermagnetic MnTe, *npj Spintronics* **2**, 45 (2024).
- [60] T. Osumi, S. Souma, T. Aoyama, K. Yamauchi, A. Honma, K. Nakayama, T. Takahashi, K. Ohgushi, and T. Sato, Observation of a giant band splitting in altermagnetic MnTe, *Phys. Rev. B* **109**, 115102 (2024).
- [61] N. Doiron-Leyraud, C. Proust, D. LeBoeuf, J. Levallois, J.-B. Bonnemaison, R. Liang, D. Bonn, W. Hardy, and L. Taillefer, Quantum oscillations and the fermi surface in an underdoped high- T_c superconductor, *Nature* **447**, 565 (2007).
- [62] S. E. Sebastian, N. Harrison, and G. G. Lonzarich, Towards resolution of the fermi surface in underdoped high- T_c superconductors, *Reports on progress in Physics* **75**, 102501 (2012).
- [63] Z.-X. Li, X. Wan, and W. Chen, Diagnosing altermagnetic phases through quantum oscillations, *arXiv preprint arXiv:2406.04073v1* (2024).
- [64] A. McCollam, S. R. Julian, P. Rourke, D. Aoki, and J. Flouquet, Anomalous de Haas-van Alphen Oscillations in CeCoIn_5 , *Physical review letters* **94**, 186401 (2005).
- [65] V. Leeb and J. Knolle, Theory of difference-frequency quantum oscillations, *Physical Review B* **108**, 054202 (2023).

- [66] V. Leeb, N. Huber, C. Pfleiderer, J. Knolle, and M. A. Wilde, A field guide to non-onsager quantum oscillations in metals, [arXiv preprint arXiv:2408.15092](#) (2024).
- [67] J. A. Ouassou, A. Brataas, and J. Linder, dc josephson effect in altermagnets, *Phys. Rev. Lett.* **131**, 076003 (2023).
- [68] C. Sun, A. Brataas, and J. Linder, Andreev reflection in altermagnets, *Phys. Rev. B* **108**, 054511 (2023).
- [69] F. Ferrari and R. Valentí, Altermagnetism on the shastry-sutherland lattice, *Physical Review B* **110**, 205140 (2024).
- [70] D.-F. Shao, S.-H. Zhang, M. Li, C.-B. Eom, and E. Y. Tsymbal, Spin-neutral currents for spintronics, *Nature Communications* **12**, 7061 (2021).
- [71] R. González-Hernández, L. Šmejkal, K. Výborný, Y. Yahagi, J. Sinova, T. c. v. Jungwirth, and J. Železný, Efficient electrical spin splitter based on nonrelativistic collinear antiferromagnetism, *Phys. Rev. Lett.* **126**, 127701 (2021).
- [72] S.-B. Zhang, L.-H. Hu, and T. Neupert, Finite-momentum cooper pairing in proximitized altermagnets, *Nature Communications* **15**, 1801 (2024).
- [73] D. Zhu, Z.-Y. Zhuang, Z. Wu, and Z. Yan, Topological superconductivity in two-dimensional altermagnetic metals, *Physical Review B* **108**, 184505 (2023).
- [74] D. Chakraborty and A. M. Black-Schaffer, Zero-field finite-momentum and field-induced superconductivity in altermagnets, *Physical Review B* **110**, L060508 (2024).
- [75] G. Sim and J. Knolle, Pair density waves and supercurrent diode effect in altermagnets, [arXiv preprint arXiv:2407.01513](#) (2024).
- [76] M. Dürrnagel, H. Hohmann, A. Maity, J. Seufert, M. Klett, L. Klebl, and R. Thomale, Altermagnetic phase transition in a lieb metal, to be submitted.
- [77] J. P. Perdew, K. Burke, and M. Ernzerhof, Generalized gradient approximation made simple, *Phys. Rev. Lett.* **77**, 3865 (1996).